ICAS 2016
30th Congress of the International Council of the Aeronautical Sciences
DCC, Daejeon, Korea ; September 25-30, 2016

# A MESH-LESS METHOD FOR COMPRESSIBLE FLOW CALCULATIONS AT ALL SPEED CONDITIONS

**A. Jahangirian*, S. Sattarzadeh***

***Aerospace Engineering Department**
**Amirkabir University of Technology, 424 Hafez Avenue, Tehran, Iran**

**Keywords**: Mesh-less method, Compressible Flow, Implicit method, Euler Equations

## Abstract

*An implicit mesh-less method is developed for solution of the compressible flows around 2D and 3D geometries. The algorithm is applied directly to the differential form of the governing equations by using least-square formulation. A dual-time implicit time discretization scheme is developed and the computational efficiency is enhanced by adopting accelerating techniques such as local time stepping, residual smoothing and enthalpy damping. The capabilities of the method are demonstrated by flow computations at subsonic, transonic and supersonic flow conditions around different geometries.*

## 1. Introduction

Increasing the power of computers during last few years, the flow simulations over complex geometries has become more viable. One of the major problems is the ability to generate high quality meshes. This is really important particularly when more sophisticated geometrics are concerned. Mesh-less methods are proposed that use point clouds instead of rigid domain discretization [1]. Finite point method (FPM) is developed by Onate et al. [2] using a polynomial basis. Katz and Jameson presented a mesh-less method based on CUSP (Convective Upwind and Split Pressure) scheme to compute inviscid flows in two dimensions in subsonic and transonic regimes [3]. The problem with mesh-less methods is the computational cost. At any iteration the computational cost of mesh-less methods is higher than mesh based ones [4]. However it is shown that the convergence history of most of mesh-less methods is better than mesh-base ones [4]. It is notable to mention that compared with mesh based algorithms; mesh-less methods have more applications, especially in the large deformations since it argues that moving points are easier than replacing the edges.

The main objective of the present study is to develop an efficient mesh-less method to solve the Euler (inviscid) equations at all speed conditions (subsonic, transonic, supersonic speed). The accuracy and the computational efficiency of the method in different flow condition is investigated, in this paper.

## 2. Numerical Method

Three-dimensional Euler equations consisting the mass, momentum, and energy conservation laws can be written in the differential form as [5]:

$$\frac{\partial Q}{\partial t}+\frac{\partial F}{\partial x}+\frac{\partial G}{\partial y}+\frac{\partial K}{\partial z}=0 \qquad (1)$$

Where:

$$Q=\begin{pmatrix}\rho\\ \rho u\\ \rho v\\ \rho w\\ \rho E\end{pmatrix},\ F=\begin{pmatrix}\rho u\\ \rho u^2+P\\ \rho vu\\ \rho wu\\ \rho Eu+Pu\end{pmatrix},$$

$$G=\begin{pmatrix}\rho v\\ \rho uv\\ \rho v^2+P\\ \rho wv\\ \rho Ev+Pv\end{pmatrix},\ K=\begin{pmatrix}\rho w\\ \rho uw\\ \rho vw\\ \rho w^2+P\\ \rho Ew+Pw\end{pmatrix} \qquad (2)$$

Here $P, \circ, u, v, w$ and $E$ are the pressure, density, Cartesian velocity components and total energy. In this work the flow equations are solved in the conservation form. A least-square formulation is used for calculating the derivatives [3]. Assume $\ddot{}_{ij}$ is the value of any function $\ddot{}$ at the mid-point of the edge ij, where j is in cloud of point i. Assuming this function varies linearly along the edge ij and using Taylor's formula about i to any of its cloud points:

$$\left(\frac{\partial \¤}{\partial x}\right)_i \Delta x_{ij} + \left(\frac{\partial \¤}{\partial y}\right)_i \Delta y_{ij} + \left(\frac{\partial \¤}{\partial z}\right)_i \Delta z_{ij} = \Delta \¤_{ij},\ \Delta x_{ij} = x_j - x_i \ , \quad \Delta y_{ij} = y_j - y_i \ , \quad \Delta z_{ij} = z_j - z_i \ , \quad \Delta \¤_{ij} = \¤_j - \¤_i \tag{3}$$

Similar equations could be written for all cloud points associated with point i subject to an arbitrary weighting factor $\mu_i$. This yields the following non-square matrix:

$$\begin{pmatrix} \mu_{i1}\Delta x_{i1} & \mu_{i1}\Delta y_{i1} & \mu_{i1}\Delta z_{i1} \\ ..... & ..... & ..... \\ \mu_{im}\Delta x_{im} & \mu_{im}\Delta y_{im} & \mu_{im}\Delta z_{im} \end{pmatrix} \begin{bmatrix} \left.\frac{\partial \¤}{\partial x}\right|_i \\ \left.\frac{\partial \¤}{\partial y}\right|_i \\ \left.\frac{\partial \¤}{\partial z}\right|_i \end{bmatrix} = \begin{bmatrix} \mu_{i1}\Delta \¤_{i1} \\ ..... \\ \mu_{im}\Delta \¤_{im} \end{bmatrix}, \quad \mu_{ij} = \frac{1}{d_{ij}^{\,q}} \tag{4}$$

Where $d_{ij}$ is the distance between point i and its neighbors. In this work q is equal one. The spatial derivatives of the function $\ddot{}$ can then be obtained by solving Eq. 3 using the least-squares method [4]:

$$\left.\frac{\partial \¤}{\partial x}\right|_i = \sum_{j=1}^{m} a_{ij}\Delta \¤_{ij} \ , \quad \left.\frac{\partial \¤}{\partial y}\right|_i = \sum_{j=1}^{m} b_{ij}\Delta \¤_{ij} \ , \quad \left.\frac{\partial \¤}{\partial z}\right|_i = \sum_{j=1}^{m} c_{ij}\Delta \¤_{ij} \tag{5}$$

The coefficients in Eq. 5 can be calculated using inverse distance weighting function as:

$$a_{ij} = \sim_{ij,1} - \frac{r_{12}}{r_{11}}\sim_{ij,2} + \ \sim_{ij,3}, \quad b_{ij} = \sim_{ij,2} - \frac{r_{23}}{r_{22}}\sim_{ij,3}, \quad c_{ij} = \sim_{ij,3} \tag{6}$$

Where the parameters are equal to:

$$r_{11} = \sqrt{\sum_{j=1}^{n} \mu_{ij}\left(\Delta x_{ij}\right)^2}, \quad r_{12} = \frac{1}{r_{11}}\sum_{j=1}^{n} \mu_{ij}\Delta x_{ij}\Delta y_{ij}$$

$$r_{22} = \sqrt{\sum_{j=1}^{n} \mu_{ij}\left(\Delta y_{ij}\right)^2 - {r_{12}}^2}, \quad r_{13} = \frac{1}{r_{11}}\sum_{j=1}^{n} \mu_{ij}\Delta x_{ij}\Delta z_{ij},$$

$$r_{23} = \frac{1}{r_{22}}\left(\sum_{j=1}^{n} \mu_{ij}\Delta y_{ij}\Delta z_{ij} - \frac{r_{12}}{r_{11}}\sum_{j=1}^{n} \mu_{ij}\Delta x_{ij}\Delta z_{ij}\right), \tag{7}$$

$$r_{33} = \sqrt{\sum_{j=1}^{n} \mu_{ij}\left(\Delta z_{ij}\right)^2 - \left({r_{13}}^2 + {r_{23}}^2\right)}$$

$$\sim_{ij,1} = \frac{\Delta x_{ij}}{{r_{11}}^2}, \quad \sim_{ij,2} = \frac{1}{{r_{22}}^2}\left(\Delta y_{ij} - \frac{r_{12}}{r_{11}}\Delta x_{ij}\right),$$

$$\sim_{ij,3} = \frac{1}{{r_{33}}^2}\left(\Delta z_{ij} - \frac{r_{23}}{r_{22}}\Delta y_{ij} + \ \Delta x_{ij}\right)$$

Applying the least-square approximations given by Eq. 5 to each component of flux functions in Eq. 1, a semi-discrete form of the Euler Equations at point i is obtained:

$$\left[\frac{\partial \mathbf{w}_i}{\partial t}\right] + \left[\sum_{j=1}^{m} a_{ij}(F_j - F_i) + \sum_{j=1}^{m} b_{ij}(G_j - G_i) + \sum_{j=1}^{m} c_{ij}(K_j - K_i)\right] = 0 \tag{8}$$

Then we define a Flux $H = aF + bG + cK$ in the direction of the least-square coefficient vector for an edge ij. The approximation of Eq. 8 with the directed flux becomes:

$$\frac{\partial W_i}{\partial t} + \sum_{j=1}^{m} \Delta H_{ij} = 0, \quad \Delta H_{ij} = H_j - H_i \tag{9}$$

It leads to the central differencing method which is unstable schemes, and must be stabled by stabilizing terms. This can be achieved by adding directly second and fourth order damping terms. In this dissipation model an aggregation of the second and fourth differences of conserved variables (W) is added in order to prevent the oscillations especially in the critical zones.

$$\frac{\partial W_i}{\partial t} + 2\sum_{j=1}^{m} \Delta H_{i\,j+1/2} - D_i = 0 \tag{10}$$

These dissipation terms are defined by:

$$D_i = \left(\nabla\left(£^{(2)a}\right)\nabla W - \nabla^2\left(£^{(4)a}\right)\nabla^2 W\right)_i, \quad (11)$$

$$\nabla\left(£^{(2)a}\right)\nabla W = \sum_{j=1}^{n}\left[\left(£^{(2)a}\right)_{i,j/2}\left(W_j - W_i\right)\right],$$

$$\nabla^2 W = \sum_{j=1}^{n}\left(W_j - W_i\right)$$

Where $£^{(2)}$ and $£^{(4)}$ are local adaptive coefficients which use the pressure as a sensor to explore sharp gradients. They are formulated as:

$$£_{ij}^{(2)} = k^{(2)}¬_{ij}, \quad £_{ij}^{4} = \max\left(0, k^{(4)} - £_{ij}^{(2)}\right),$$

$$¬_{ij} = \frac{\left|P_j - P_i\right|}{\left|P_j + P_i\right|} \quad (12)$$

The $k_2$ parameter is introduced to prevent the oscillations near shock waves while $k_4$ is added to suppress the oscillations in the remaining part of the domain. The values of the constant $k_2$ and $k_4$ are in the range $0 < k_2 < 1$ and $\frac{1}{256} < k_4 < \frac{1}{20}$ [1] and $¬_{ij}$ is a pressure sensor for shocks at any ij edges. $a_{ij}$ is defined as the largest eigenvalue equals the flux Jacobian matrix ($\frac{\partial F}{\partial W}$ and $\frac{\partial G}{\partial W}$ and $\frac{\partial K}{\partial W}$) which are relevant to the Euler equations [4]. Applying Eq. 10 to each node in the computational domain, the result will be a set of ordinary differential equations in an implicit form in the following form:

$$\frac{\partial W_i}{\partial t} + R\left(W_i\right) = 0, R\left(W_i\right) = \sum_{j=1}^{m}\Delta H_{ij} - D_i \quad (13)$$

$$, \frac{dW}{dt} + R\left(W_i^{n+1}\right) = 0$$

The explicit four-stage Runge–Kutta method is used for time discretisation in this study. In the present work a second order accurate time discretization is used. At this stage it is beneficial to redefine a new residual $R^*$, referred to as unsteady residual.

$$\frac{3W_i^{n+1}}{2\Delta t} - \frac{-2W_i^{n}}{\Delta t} + \frac{W_i^{n-1}}{2\Delta t} + R\left(W_i^{n+1}\right) = 0, \quad (14)$$

$$R^*\left(W_i^{n+1}\right) = \frac{3W_i^{n+1}}{2\Delta t} - \frac{-2W_i^{n}}{\Delta t} + \frac{W_i^{n-1}}{2\Delta t} + R\left(W_i^{n+1}\right)$$

The new equation can be considered as the solution of a steady-state problem which can then be solved with a time marching method by introducing a derivative with respect to a fictitious pseudo-time[2].

$$\frac{\partial W_i^{n+1}}{\partial ²} = 0,$$

$$²_i = \min\left[\frac{CFL_{expicit}}{\sum_{j=1}^{n}\left(\left(a_{ij}\bar{u} + b_{ij}\bar{v} + c_{ij}\bar{w}\right) + \bar{c}\sqrt{a_{ij}^2 + b_{ij}^2 + c_{ij}^2}\right)}, \frac{2\Delta t_i}{3}\right] \quad (15)$$

Where $²_i$ is the time step for any inner explicit iteration and $\bar{u}, \bar{v}, \bar{w}$ and $\bar{c}$ are the velocity components and speed of sound at mid-point, respectively. $CFL_{\exp}$ is the courant number for inner explicit iterations. For calculations in this work implicit and explicit CFL numbers of 100000 and 5 are used. For all test cases, the inner explicit solution iterates until the average of density residuals reaches to the level of 0.01. To accelerate the convergence residual smoothing and enthalpy damping are also used in the present work. To solve Euler equations at a solid boundary, no mass or other convective fluxes can penetrate the solid body. In the far field, characteristic analysis is used based on Riemann invariants to determine the values of the flow variables on the outer nodes [4].

## 3. Results

The capabilities of the method are demonstrated by flow computations around different 2D and 3D geometries.

A subsonic flow around NACA0012 airfoil is considered at Mach number 0.5 and angle of attack zero degree. In this case the values of 0.45 and 0.02 are used for scalar dissipation coefficients $k_2$ and $k_4$, respectively. It is noted that in all test cases CFL number, Runge-Kutta and residual smoothing coefficients are fixed [4]. The point distribution is shown in Fig. 1. The domain includes 6509 points in which 280 points are on the solid boundary and 60 points are on the outer boundary. In this test, explicit

CFL number of 5 and implicit CFL number of 100000 are used. The surface pressure coefficient distributions are shown in Fig. 2. As it is seen, the results are in good agreements with the finite volume method [5] confirming the acceptable accuracy of the presented mesh-less method. Convergence history for this case is shown in Fig.3, demonstrating that the computational efficiency of the implicit mesh-less method is much better than the explicit approach as expected. The computations are done on a Pentium PC Dual core with 2.00 GHz speed.

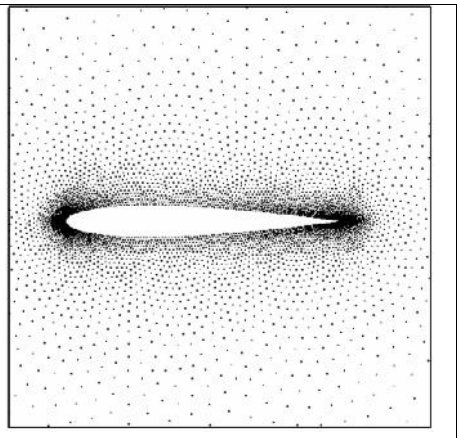

**Fig. 1. Point distribution over NACA0012**

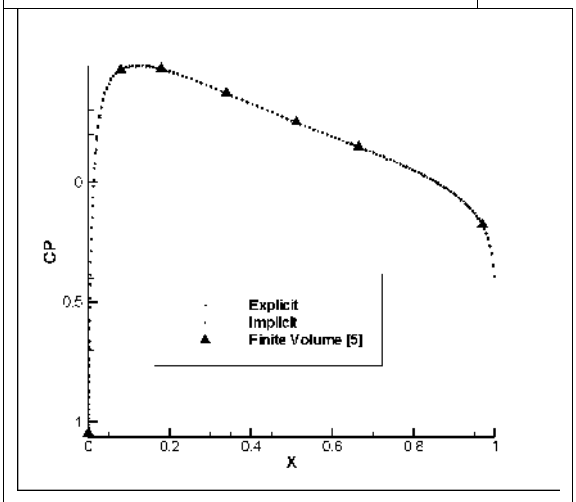


**Fig.2. Surface pressure coefficients at M= 0.5 and AOA= 0.**

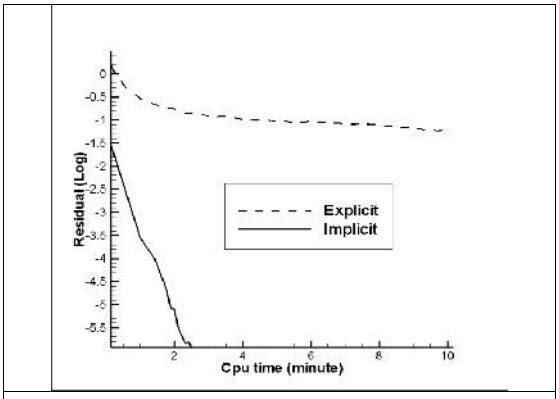


**Fig.3. Convergence history for NACA 0012 airfoil at M =0.5 and AOA= 0.**

The next case is an inviscid flow at transonic flow conditions of M=0.8, AOA=1.25. The point distribution is the same as the previous case. The pressure contour is shown in figures 4. As illustrated in this figure the shock wave is well resolved.

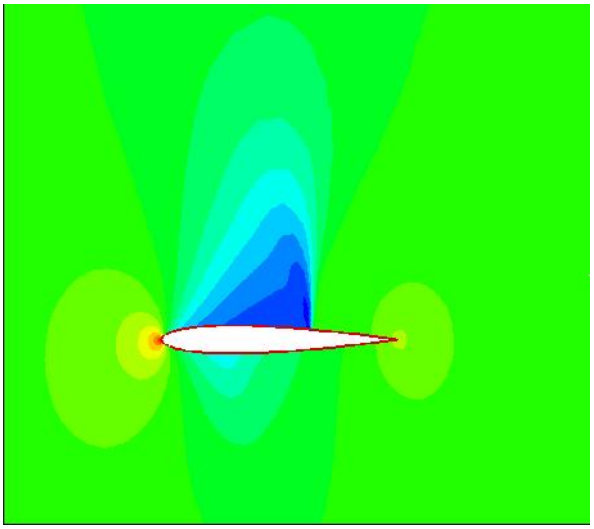

**Fig. 4. The pressure contour over NACA0012 airfoil at M =0.5 and AOA= 0.**

The surface pressure coefficient distributions are shown in figure 5 (a). As illustrated the results are in good agreement with the referenced finite volume data [5] specially, in capturing the shock wave. In figure 5 (b) the convergence history is shown. As illustrated implicit method has better convergence in comparison with explicit method.

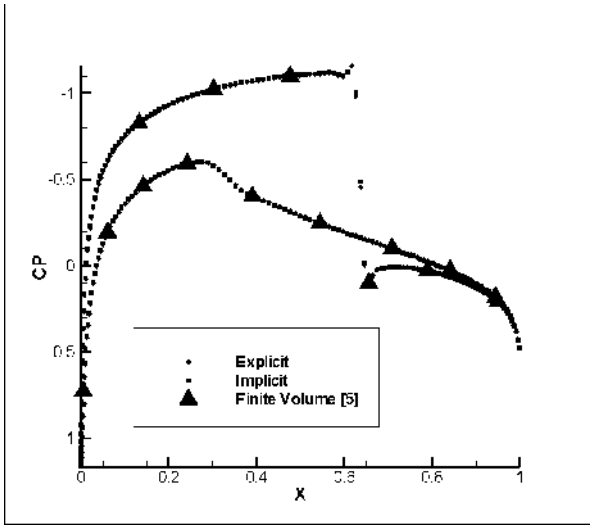


**(a)**

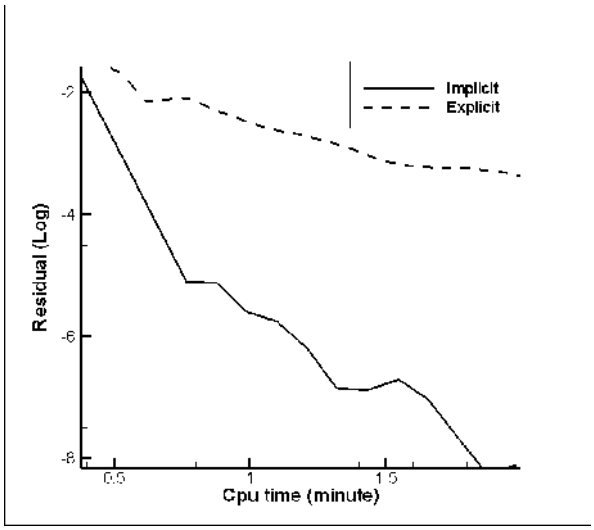


**(b)**

**Fig.5. (a) Surface pressure coefficients (b) Convergence history at M= 0.8 and AOA= 1.25**

The third case is a supersonic flow one that is defined to show the potential of the presented method to simulate the flows at higher speed conditions. The flow conditions are $M_\infty = 1.2$ , $\sim = 10.00^o$ over NACA 0012 airfoil. The point distribution is the same as the first case. The surface pressure coefficient distributions are compared with other numerical results of reference [5] in Fig. 6. As illustrated, good agreements are obtained.

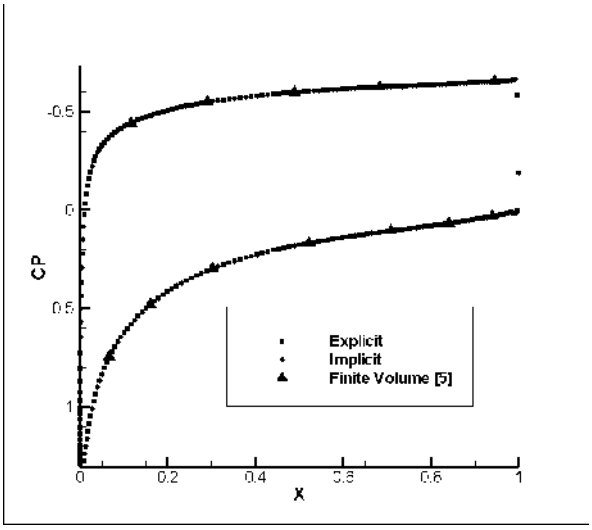


**Fig.6. Surface pressure coefficient and at** $M_\infty = 1.20$ , $\sim = 10^o$

The next case is the subsonic flow around a typical helicopter with the Mach number 0.3. There are 121752 points in the domain in which 12925 points are in the surface of the helicopter. The point distribution in the middle section is shown in Fig. 7.a. The pressure contours in the middle section is shown in Fig. 7.b. As it is shown, smooth results in different sections are achieved.

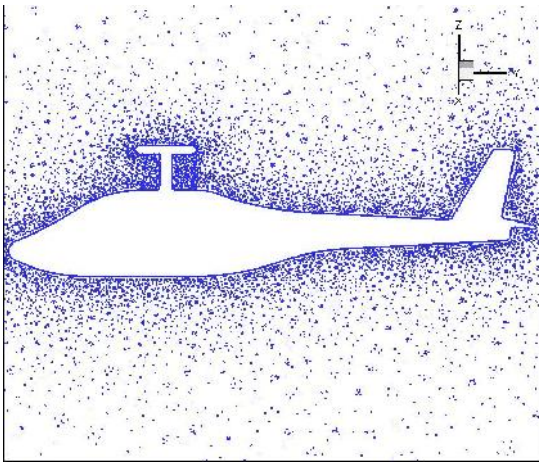

(a)

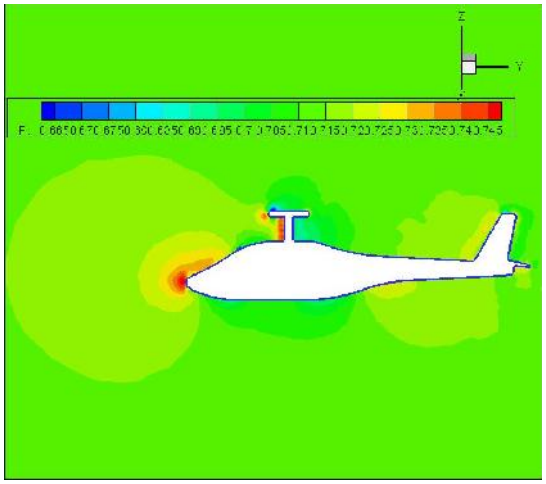

(b)

**Fig 7.a) Point distribution b) Pressure contours in the middle section**

The last test case is defined to show the ability of the mesh-less method to simulate the transonic flow over ONERA M6 wing. The flow conditions are $M_\infty = 0.8395$ , $\sim = 3.06^o$. The surface point distribution is shown in Fig. 8. There are 145496 points in the domain from those 22958 points are on the solid boundary.

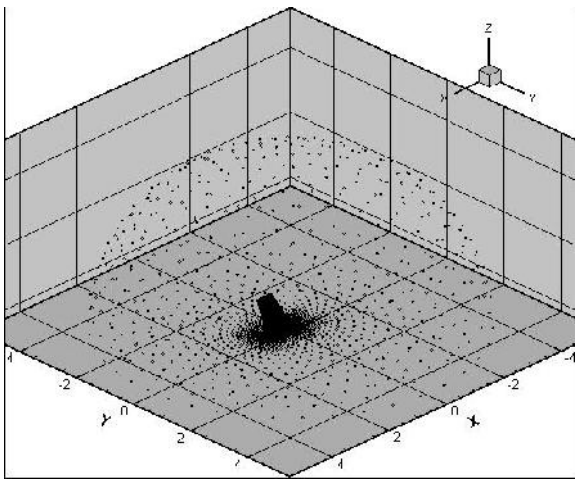

(a)

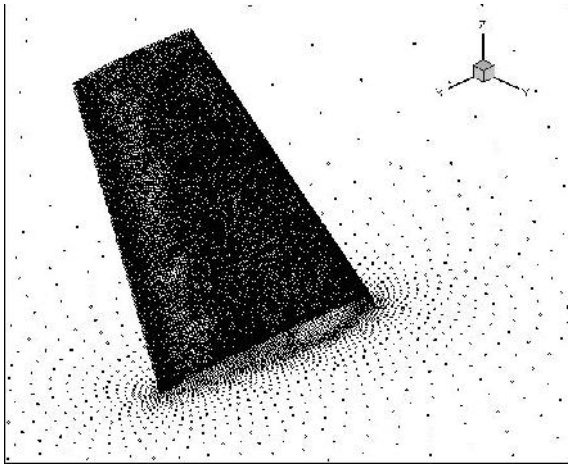

(b)

**Fig 8. Point distribution over ONERA M6 wing.**

The surface pressure distribution at section z/b=0.9 is compared with the experimental data [6] in Fig. 9.a. The surface pressure contours are demonstrated in Fig. 9.b.which the shock wave moving from the backward of the wing at the root sections to the forward locations at the tip sections.

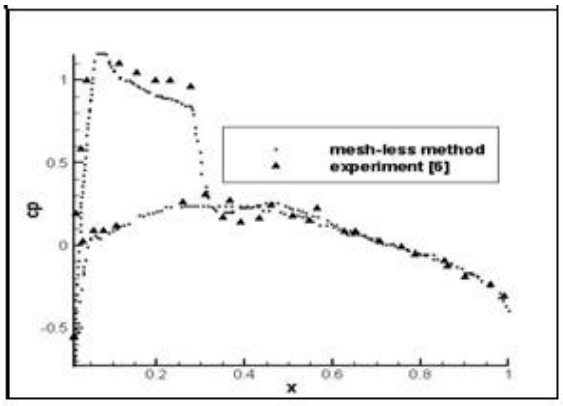


**a) Pressure coefficient (ONERA M6 z/b=0.9)**

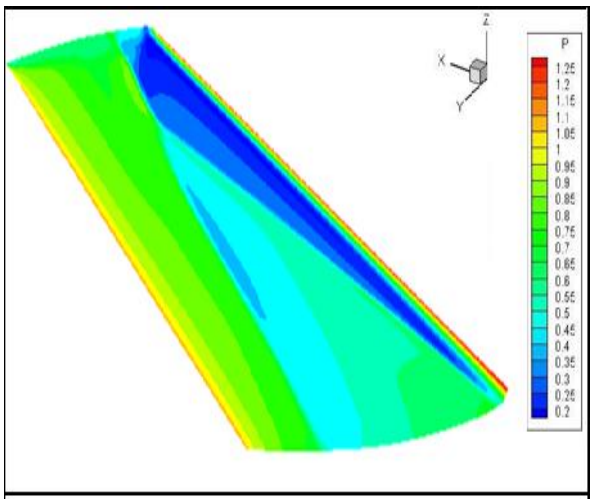


**b) Pressure contours**

**Fig. 9 results at** $M_\infty = 0.8395$ , $\sim = 3.06^o$.

## 3. Summery

An implicit mesh-less method was developed to calculate the compressible flows around 3D geometries. The capabilities of the method were shown by flow computations at all speed conditions around 3D geometries. Results were presented which had good agreements with experimental and other reliable numerical data. The method was shown to reduce the computational time by about 50% compared with the alternative explicit method.

## References

[1] Katz A and Jameson A, A Comparison of Various Meshless Schemes within a Unified Algorithm, *47th AIAA Aerospace Sciences Meeting including The New Horizons Forum and Aerospace Exposition*, Orlando, Florida, 2009.

[2] Onate E, Idelsohn S, Zienkiewicz C, Taylor L and Sacco C, A Stabilized Finite Point Meth. for Analysis of Fluid Mech. *Prob., Comp. Meth. Appl. Mech. Energy*, vol.139, pp 315-346, 1996.

[3] Katz A and Jameson A, Edge-based Meshless Methods for Compressible Flow Simulations, *46th AIAA Aerospace Sciences Meeting and Exhibit*, Reno, Nevada, 2008.

[4] Jahangirian A and Hashemi Y, An Efficient Implicit Mesh-less Method for Compressible Flow Calculations, *Int. J. for Num. Meth. in Fluids*, Vol. 67, No. 6, pp 754-770, 2011.

[5] Jameson A, and Mavriplis D, Finite Volume Solution of the Two-Dimensional Euler Equation on a Regular Triangular Mesh, *AIAA Journal*, Vol. 24 pp 611-618, 1986.

[6] Schmitt V, Charpin F, Pressure Distributions on the ONERA-M6 Wing at Transonic Mach Numbers, Experimental Data Base for Computer Program Assessment. *Report of the Fluid Dynamics Panel, Working Group 04, AGARD AR* 138, 1979.

## Contact Author Email Address

ajahan@aut.ac.ir

## Copyright Statement